A Transversely Isotropic Biphasic Model for Unconfined Compression of Growth Plate and Chondroepiphysis

B. Cohen[1]

W. M. Lai

V. C. Mow

Departments of Mechanical Engineering and Orthopaedic Surgery, Columbia University, New York, NY 10032

Using the biphasic theory for hydrated soft tissues (Mow et al., 1980) and a transversely isotropic elastic model for the solid matrix, an analytical solution is presented for the unconfined compression of cylindrical disks of growth plate tissues compressed between two rigid platens with a frictionless interface. The axisymmetric case where the plane of transverse isotropy is perpendicular to the cylindrical axis is studied, and the stress-relaxation response to imposed step and ramp displacements is solved. This solution is then used to analyze experimental data from unconfined compression stress-relaxation tests performed on specimens from bovine distal ulnar growth plate and chondroepiphysis to determine the biphasic material parameters. The transversely isotropic biphasic model provides an excellent agreement between theory and experimental results, better than was previously achieved with an isotropic model, and can explain the observed experimental behavior in unconfined compression of these tissues.

Introduction

The growth plate (physis) of immature long bones is the thin (≅2 mm) cartilaginous plate that separates the shaft from the bony end (epiphysis). Proliferative and hypertrophic chondrocytes are organized in columns whose orientation defines the axis of longitudinal bone growth (Brighton, 1978; Buckwalter et al., 1985; Hunziker et al., 1987), surrounded by collagen-rich fibrous extracellular matrix (Speer, 1982). The pre-ossific cartilage adjacent to the growth plate in the epiphysis of immature long bones is termed chondroepiphysis, Fig. 1. The form of the growth plate has been thought to follow a pattern most suited to produce primarily a state of compression within the tissue (Smith, 1962; Carter et al., 1987) under normal load bearing, which is considered vital for growth and development. Excessive compression, however, can be detrimental and lead to growth abnormalities (Letts, 1988). This has been the motivation for a number of biomechanical studies on the growth plate (Bright et al., 1974; Cohen et al., 1994; Moen and Pelker, 1984).

The mechanical behavior of hydrated soft tissues such as articular cartilage has been successfully described by the biphasic theory (Mow et al., 1980) where the tissue is modeled as a mixture of two distinct, homogeneous, immiscible, and intrinsically incompressible phases: an elastic isotropic solid and an inviscid fluid. Fluid flow and solid deformation are coupled through a momentum exchange term, linearly proportional to the relative velocity of the two phases, which is responsible for the description of the time-dependent (viscoelastic) deformational behavior. The intrinsic biphasic material properties are determined by standard experimental procedures such as uniaxial (confined) compression, unconfined compression and indentation (Armstrong et al., 1984; Mow et al., 1980; Mak et al., 1987).

The unconfined compression test was used to study the mechanical behavior and load effects of hydrated soft tissues such as articular cartilage (Armstrong et al., 1984; Mizrahi et al., 1986), growth plate and chondroepiphysis (Brown and Singerman, 1986; Gray et al., 1988; Kim et al., 1995), and cardiac muscle (Yang and Taber, 1991). Armstrong et al. (1984) also obtained a theoretical solution (assuming infinitesimal deformation, frictionless platen interfaces, and isotropic material properties) and reported that a good agreement between the theoretical response and experimental data could not be obtained. They attributed this to confinement effects due to surface adhesion at the tissue-platen interface. Brown and Singerman (1986) reported obtaining only limited accuracy in curve-fitting the experimental data, which presented a much higher peak stress and more rapid relaxation time than the theoretical prediction of the Armstrong et al. (1984) solution. Spilker et al. (1990) studied the effects of friction at the tissue-platen interface in unconfined compression with use of the finite element formulation of the biphasic theory (Spilker and Suh, 1990) and showed that it can explain only part of the theory–experiment discrepancy reported by Armstrong et al. (1984) and observed by Brown and Singerman (1986). Another possible explanation could be the intrinsic bulk viscoelasticity of the solid matrix of the tissue (Mak, 1986). The analysis by Lanir (1987) of the unconfined compressive response of a transversely isotropic cartilage disk included the apparent effect of osmotic pressure, and was used to explain the "instantaneous" response described in the experiments of Mizrahi et al. (1986).

In this study we propose that the dramatic stress-relaxation behavior (high peak stress and rapid relaxation time) observed experimentally in unconfined compression is due to the restraining (confining) effect of extracellular matrix against lateral (radial) displacement producing tensile strains in the transverse plane (with a much higher tensile stiffness) and that this behavior can be described by a transversely isotropic biphasic model.

Theoretical Formulation

Basic Equations. In the biphasic theory (Mow et al., 1980), the stress–strain relations for the solid matrix, the interstitial fluid, and the total stress are given, respectively, by

[1] Current address: RAFAEL, Haifa 31021, Israel.

Contributed by the Bioengineering Division for publication in the JOURNAL OF BIOMECHANICAL ENGINEERING. Manuscript received by the Bioengineering Division December 10, 1995; revised manuscript received February 12, 1998. Associate Technical Editor: R. C. Haut.

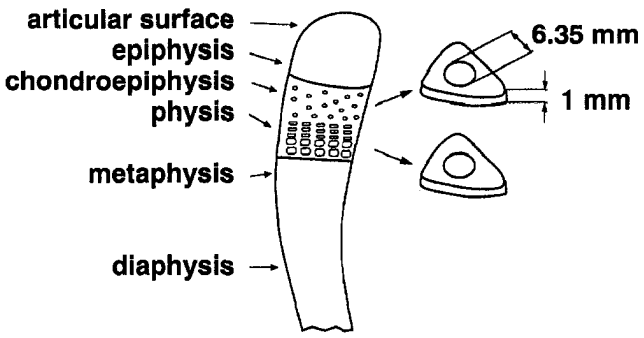

Fig. 1 Specimen preparation from the 4 month old bovine distal ulna, showing the two sections representing growth plate (columnar region) and chondroepiphysis

$$\boldsymbol{\sigma}^s = -\phi^s p\mathbf{I} + \boldsymbol{\sigma}^E, \tag{1a}$$

$$\boldsymbol{\sigma}^f = -\phi^f p\mathbf{I}, \tag{1b}$$

$$\boldsymbol{\sigma}^t = \boldsymbol{\sigma}^s + \boldsymbol{\sigma}^f = -p\mathbf{I} + \boldsymbol{\sigma}^E, \tag{1c}$$

where p is the pressure, ϕ^s and ϕ^f are the volume fractions for the solid and fluid phases, respectively, and $\boldsymbol{\sigma}^E$ is the elastic stress tensor of the solid matrix. For the anisotropic, linearly elastic material the infinitesimal strain tensor, $\boldsymbol{\epsilon}$, is related to $\boldsymbol{\sigma}^E$ by $\boldsymbol{\sigma}^E = \underline{\mathbf{C}} \cdot \boldsymbol{\epsilon}$ where $\underline{\mathbf{C}}$ is a fourth-order stiffness tensor. For an isotropic material, the linear elastic stress–strain law becomes $\boldsymbol{\sigma}^E = \lambda_s e\mathbf{I} + 2\mu_s\epsilon$, where $e = \mathrm{tr}\epsilon$ is the infinitesimal dilatation, and λ_s and μ_s are the Lamé constants. For a material that is transversely isotropic about the e_3 axis and for axisymmetric problems about the e_3 axis, the nonzero elastic stress and the strain tensors may be written in contracted vector forms related through a 4×4 stiffness matrix as (Jones, 1975)

$$\begin{pmatrix} \sigma_{rr} \\ \sigma_{\theta\theta} \\ \sigma_{zz} \\ \sigma_{zr} \end{pmatrix} = \begin{bmatrix} C_{11} & C_{12} & C_{13} & 0 \\ C_{12} & C_{11} & C_{13} & 0 \\ C_{13} & C_{13} & C_{33} & 0 \\ 0 & 0 & 0 & C_{44} \end{bmatrix} \begin{pmatrix} \epsilon_{rr} \\ \epsilon_{\theta\theta} \\ \epsilon_{zz} \\ 2\epsilon_{zr} \end{pmatrix}. \tag{2}$$

where (r, θ, z) are cylindrical coordinates and the $r-\theta$ plane is the plane of isotropy. The five independent components of the stiffness matrix can be written in terms of Young's moduli and Poisson's ratios in the transverse plane (E_1 and $\nu_{21} = \nu_{12}$), and out-of-plane (E_3 and $\nu_{31} = \nu_{13}E_3/E_1$), and the out-of-plane shear modulus G_{31}, as follows

$$C_{11} = E_1(1 - \nu_{31}^2 E_1/E_3)/[(1 + \nu_{21})\Delta_1] \tag{3a}$$

$$C_{12} = E_1(\nu_{21} + \nu_{31}^2 E_1/E_3)/[(1 + \nu_{21})\Delta_1] \tag{3b}$$

$$C_{13} = E_1\nu_{31}/\Delta_1 \tag{3c}$$

$$C_{33} = E_3[1 + 2\nu_{31}^2(E_1/E_3)/\Delta_1] \tag{3d}$$

$$C_{44} = G_{31}, \tag{3e}$$

where $\Delta_1 \equiv 1 - \nu_{21} - 2\nu_{31}^2 E_1/E_3$. (Note that in this case, Poisson's ratio is defined by the ratio of transverse strain ϵ_{jj} to axial strain ϵ_{ii} in response to uniaxial stress σ_{ii}, i.e., $\nu_{ij} = -\epsilon_{jj}/\epsilon_{ii}$.)

With both phases considered intrinsically incompressible and homogeneous in the undeformed state, the continuity equation is given by

$$\nabla \cdot (\phi^s \mathbf{v}^s + \phi^f \mathbf{v}^f) = 0. \tag{4}$$

Neglecting inertia effects, the momentum equations for the solid and fluid phases are, respectively,

$$-\phi^s \nabla p + \nabla \cdot \boldsymbol{\sigma}^E + K(\mathbf{v}^f - \mathbf{v}^s) = \mathbf{0}, \tag{5a}$$

$$-\phi^f \nabla p - K(\mathbf{v}^f - \mathbf{v}^s) = \mathbf{0}, \tag{5b}$$

$$\nabla \cdot \boldsymbol{\sigma}^t = \mathbf{0}. \tag{5c}$$

where $\mathbf{v}^s$ and $\mathbf{v}^f$ are the velocities of the solid and fluid phases, respectively, and K is the diffusive drag coefficient, related to the permeability k by $K = (\phi^f)^2/k$ (Lai and Mow, 1980).

Definition of the Unconfined Compression Problem. In unconfined compression tests, a thin cylindrical disk is compressed between two rigid impermeable and smooth platens, and is free to expand radially (Fig. 2). Radial expansion is unconstrained, and free fluid flow is enabled across the cylindrical boundary surface. Either load (creep test) or displacement (stress-relaxation test) can be imposed in the axial direction. Here, we assume that the disk of tissue is transversely isotropic with E_1 being Young's modulus (in tension) in the transverse plane and E_3 Young's modulus (in compression) in the axial direction. Following Armstrong et al. (1984) we assume the solid displacement u_r, u_z, the fluid velocity v_r^f, and the pressure p to be of the form: $u_r = u(r, t)$, $v_r^f = v^f(r, t)$, $p = p(r, t)$, $u_z = z\epsilon(t)$, where $\epsilon(t)$ is the time-dependent uniform axial strain. The nonzero strain components are: $\epsilon_{rr} = \partial u/\partial r$, $\epsilon_{\theta\theta} = u/r$, $\epsilon_{zz} = \epsilon$. Under the specified conditions, the following differential equations can be obtained for the radial displacement and the pressure, respectively:

$$\frac{\partial^2 u}{\partial r^2} + \frac{1}{r}\frac{\partial u}{\partial r} - \frac{u}{r^2} = \frac{1}{C_{11}k}\frac{\partial}{\partial t}\left(u + \frac{r}{2}\epsilon\right) \tag{6}$$

$$\frac{\partial p}{\partial r} = \frac{1}{k}\frac{\partial}{\partial t}\left(u + \frac{r}{2}\epsilon\right). \tag{7}$$

Nomenclature

a = disk radius
$\mathbf{C}$ = stiffness matrix
C_i = constants
E_i = Young's modulus
f = load intensity (applied force per unit undeformed area)
$H(t)$ = Heavyside step function
H_A = aggregate modulus
I_0, I_1 = modified Bessel functions of the first kind
$\mathbf{I}$ = unity tensor
J_0, J_1 = Bessel functions of the first kind
K = diffusive drag coefficient
k = permeability
p = fluid pressure
s = Laplace transform variable
t = time variable
t_g = gel diffusion time
$\mathbf{u}$ = displacement vector
u = radial displacement
$\mathbf{v}$ = velocity vector
x = dummy variable
α_n = roots of Eq. (16)
Δ_i = constants
$\boldsymbol{\epsilon}$ = strain tensor
ϵ = uniform axial strain
ϵ_0 = constant strain
$\dot{\epsilon}_0$ = constant strain rate
ϕ = volume fraction
λ = Lamé constant
μ = Lamé constant
ν_{ij} = Poisson's ratio
$\boldsymbol{\sigma}$ = stress tensor

Superscripts

f = fluid phase
s = solid phase
t = total

Subscripts

eq = equilibrium

Notations

$(\ )'$ = dimensionless form of $(\ )$
$\bar{(\ )}$ = Laplace transform of $(\ )$
$r-\theta-z$ = cylindrical coordinate system

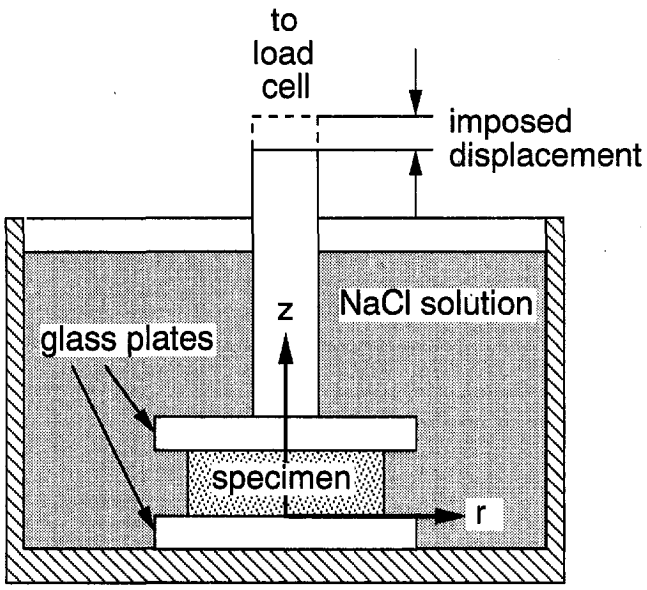

Fig. 2 Schematic of the unconfined compression test

The stress-free boundary conditions at the outer surface yield $\sigma^s_{rr} = 0$ and $p = 0$ at $r = a$, and the solution is required to be bounded at the axis of symmetry, i.e., $u = 0$ at $r = 0$. For the stress-relaxation case, $\epsilon(t)$ is a prescribed time function. The load intensity (applied force per unit undeformed area) on the platen $f(t) = [\int_0^a \sigma'_{zz}(t)2\pi r dr]/\pi a^2$, is given by

$$f(t) = \frac{2}{a^2}\int_0^a \left[-p + C_{13}\left(\frac{\partial u}{\partial r} + \frac{u}{r}\right) + C_{33}\epsilon\right] r dr. \quad (8)$$

Mathematical Solution. Let

$$r' = \frac{r}{a}, \; u' = \frac{u}{a}, \; t' = \frac{C_{11}kt}{a^2}, \; C'_{ij} = \frac{2C_{ij}}{C_{11} - C_{12}},$$

$$\sigma'_{ij} = \frac{2\sigma_{ij}}{C_{11} - C_{12}}, \; p' = \frac{2p}{C_{11} - C_{12}}. \quad (9)$$

Equations (6) and (7), together with the boundary conditions and the zero initial condition, can be easily solved by the method of Laplace transform with respect to the dimensionless time t'. The solutions of the transformed equations are given below:

$$\overline{u'} = -\frac{\bar{\epsilon} r'}{2}\left[1 - \frac{(C'_{11} + C'_{12} - 2C'_{13})I_1(\sqrt{s}r')/\sqrt{s}r'}{C'_{11}I_0(\sqrt{s}) - 2I_1(\sqrt{s})/\sqrt{s}}\right] \quad (10)$$

and

$$\overline{p'} = \frac{C'_{11}(C'_{11} + C'_{12} - 2C'_{13})}{2}\left[\frac{I_0(\sqrt{s}r') - I_0(\sqrt{s})}{C'_{11}I_0(\sqrt{s}) - 2I_1(\sqrt{s})/\sqrt{s}}\right]\bar{\epsilon}, \quad (11)$$

where a superbar denotes a transformed variable (i.e., $\overline{u'}(s)$ is the Laplace transform of u'), and I_0 and I_1 are modified Bessel functions of the first kind. The load intensity (8) becomes

$$\overline{f'} = \left[\frac{C_1 I_0(\sqrt{s}) - C_2 C_0 I_1(\sqrt{s})/\sqrt{s}}{I_0(\sqrt{s}) - C_0 I_1(\sqrt{s})/\sqrt{s}}\right]\bar{\epsilon}, \quad (12)$$

where

$$C_0 = \frac{C_{11} - C_{12}}{C_{11}}, \; C_1 = \frac{2C_{33} + C_{11} + C_{12} - 4C_{13}}{C_{11} - C_{12}},$$

and

$$C_2 = 2\frac{C_{33}(C_{11} - C_{12}) + C_{11}(C_{11} + C_{12} - 4C_{13}) + 2C_{13}^2}{(C_{11} - C_{12})^2}. \quad (13)$$

It should be noted that for the case of an isotropic solid matrix

$$C_{11} = C_{33} = \lambda_s + 2\mu_s = H_A, \quad C_{12} = C_{13} = \lambda_s,$$
$$C_{44} = \tfrac{1}{2}(C_{11} - C_{12}) = \mu_s. \quad (14)$$

In this case, $C_0 = 2\mu_s/H_A$, $C_1 = 3$ and $C_2 = 4$, and the radial displacement, pressure, and load intensity Eqs. (10)–(12) reduce to those given by Armstrong et al. (1984).

In a stress-relaxation test, the applied axial strain time history, $\epsilon(t)$, is prescribed, and the transformed load intensity, $\overline{f'}(s)$, is obtained from its Laplace transform, $\bar{\epsilon}(s)$, and Eq. (12). Alternatively, in a creep test, a load intensity $f'(t)$ is prescribed, with a Laplace transform $\overline{f'}(s)$, and the transformed axial strain $\bar{\epsilon}(s)$ is calculated from Eq. (12). Inversion of Eqs. (10)–(12) can be obtained with use of the residue theorem (Cohen, 1992).

Response to Step Displacement. For an imposed step displacement, $\epsilon = \epsilon_0 H(t)$ (where $H(t)$ is the Heavyside step function), for which $\bar{\epsilon} = \epsilon_0/s$, the inversion of Eq. (12) for the load intensity f yields:

$$f(t) = E_3\epsilon_0 + E_1\epsilon_0\Delta_3\sum_{n=1}^{\infty}\frac{\exp(-\alpha_n^2 C_{11}kt/a^2)}{\Delta_2^2\alpha_n^2 - \Delta_1/(1 + \nu_{21})}, \quad (15)$$

where $\Delta_2 \equiv (1 - \nu_{31}^2 E_1/E_3)/(1 + \nu_{21})$ and $\Delta_3 \equiv (1 - 2\nu_{31}^2)\Delta_2/\Delta_1$. α_n are roots of the transcendental equation

$$J_1(x) - \left(\frac{1 - \nu_{31}^2 E_1/E_3}{1 - \nu_{21} - 2\nu_{31}^2 E_1/E_3}\right)xJ_0(x) = 0, \quad (16)$$

in which J_0 and J_1 are Bessel functions of the first kind.

Following Armstrong et al. (1984), the short time response of the load intensity can be obtained with use of asymptotic expansions of Bessel functions for large arguments (i.e., $s \to \infty$) and the inverse Laplace transform of Eq. (12). Thus, the ratio of the peak load intensity (f_{peak}, at $t \to 0^+$) to the one at equilibrium (f_{eq}, at $t \to \infty$) can be obtained as

$$\frac{f_{\text{peak}}}{f_{eq}} = \frac{1}{2}\left[\frac{2(1 - \nu_{21}) + (1 - 4\nu_{31})E_1/E_3}{1 - \nu_{21} - 2\nu_{31}^2 E_1/E_3}\right]. \quad (17)$$

The maximum values obtained for the particular case of $\nu_{31} = 0$ are depicted in Fig. 3 for different values of ν_{21} and E_1/E_3. It should be noted that for the isotropic case, Eq. (17) reduces to $3/[2(1 + \nu)]$, which attains a maximum value of 1.5 for $\nu = 0$, as given by Armstrong et al. (1984). The load intensity at equilibrium f_{eq} and axial strain ϵ_0 in unconfined compression of the transversely isotropic case are related by the elastic modulus E_3 as

$$f_{eq} = E_3\epsilon_0. \quad (18)$$

For comparison, this relation in the case of confined compression is easily seen to be given by

$$f_{eq} = C_{33}\epsilon_0 = E_3\left(1 + \frac{2\nu_{31}^2 E_1/E_3}{1 - \nu_{21} - 2\nu_{31}^2 E_1/E_3}\right)\epsilon_0. \quad (19)$$

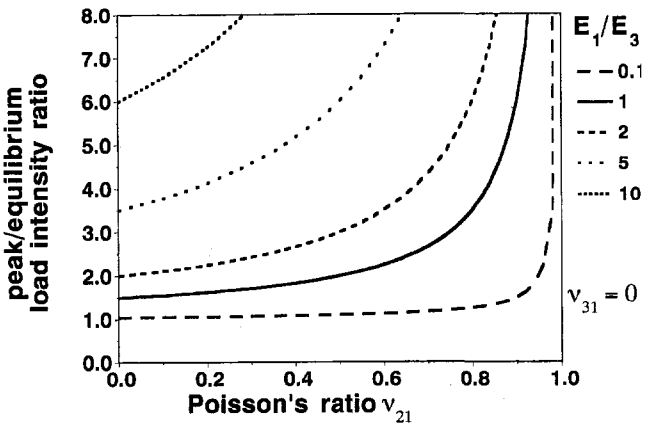

Fig. 3 The effect of ν_{21} and E_1/E_3 on the peak to equilibrium ratio of the load intensity in the stress-relaxation response to a step displacement. Note the high values that this ratio can attain (much greater than 1.5).

Response to Ramp Displacement. In a similar fashion, the load intensity response can be obtained for the case where a constant strain rate $\dot{\epsilon}_0$ is imposed until time t_0, i.e., $\epsilon(t) = \dot{\epsilon}_0[tH(t) - (t - t_0)H(t - t_0)]$ (where $H(t)$ is the Heavyside step function) as:

$$f(t) = E_3\dot{\epsilon}_0 t + E_1 \frac{\dot{\epsilon}_0 a^2}{C_{11}k}\Delta_3\left\{\frac{1}{8} - \sum_{n=1}^{\infty}\frac{\exp(-\alpha_n^2 C_{11}kt/a^2)}{\alpha_n^2[\Delta_2^2\alpha_n^2 - \Delta_1/(1+\nu_{21})]}\right\} \quad (20a)$$

for $0 < t < t_0$, and

$$f(t) = E_3\dot{\epsilon}_0 t_0 - E_1\frac{\dot{\epsilon}_0 a^2}{C_{11}k} \times \Delta_3\left\{\sum_{n=1}^{\infty}\frac{\exp(-\alpha_n^2 C_{11}kt/a^2) - \exp[-\alpha_n^2 C_{11}k(t-t_0)/a^2]}{\alpha_n^2[\Delta_2^2\alpha_n^2 - \Delta_1/(1+\nu_{21})]}\right\} \quad (20b)$$

for $t > t_0$. At equilibrium (as $t \to \infty$), the load intensity will be $f_{eq} = E_3\dot{\epsilon}_0 t_0$.

The effect of ν_{21} on the stress-relaxation time history is shown in Fig. 4(*a*) for the special case in which $\nu_{31} = 0$, $E_1/E_3 = 5$, and the ratio of the ramp time to the gel diffusion time ($t_g = a^2/C_{11}k$) is $t_0/t_g = 1$. The effect of the t_0/t_g ratio on the stress relaxation time history is illustrated in Fig. 4(*b*) for the special case of $\nu_{21} = 0.3$, $\nu_{31} = 0$, and $E_1/E_3 = 5$.

Experimental Procedure

Ten distal ulnae from 4-month-old calves were obtained within six hours of slaughter, and dissected free of all surrounding soft tissue. The epiphysis (including the physis and the chondroepiphysis) was separated from the diaphysis by sectioning along the physeal–metaphyseal interface with a sharp scalpel blade, Fig. 1. Two thin sections, about 2 mm thick each, were next obtained from the entire width of the cartilaginous region by consecutive sections. The columnar region of the bovine distal ulnar physis usually varies between 1 and 1.5 mm. Therefore, the first section (adjacent to the metaphysis) was used to obtain growth plate (GP) specimens (columnar regions), and the second section was used to obtain chondroepiphysis (CE) specimens (including reserve zone growth plate). The two sections were then trimmed to obtain parallel surfaces in the following procedure: First, the metaphyseal-side surface was placed flat on the freezing stage (Hacker Instruments, Fairfield, NJ) of a sledge microtome (Leitz, Rockleigh, NJ). The upper surface was then trimmed at 10 μm increments until it was parallel to the metaphyseal-side surface. Second, the specimen was inverted and slightly trimmed to obtain the final section with parallel surfaces and a thickness of 1 mm. Next, a circular disk, 6.35 mm in diameter, was cored from each section with a sharp tapered cutter (model 3427A11, McMaster Carr Supply Co., New Brunswick, NJ), Fig. 1. The diameter of the circular specimens was determined as an average of three measurements at 60 deg intervals using a stereomicroscope (model PP& E56939, Bausch and Lomb, Rochester, NY) equipped with a precision translation stage (model 203889, Olympus, New Hyde Park, NY) digital displacement indicator (model 1-645PX, IKL Inc., Newport Beach, CA). The thickness of each disk was measured to ± 3 μm accuracy using an apparatus that senses the conductivity of the tissue (Akizuki et al., 1986). Six measurements where taken and averaged. Each disk was subjected to two tests (order of the tests was randomized): (1) confined compression between two rigid-porous filters (Mow et al., 1980), and (2) unconfined compression between two smooth glass plates. In each test, specimens were initially preloaded in compression up to 0.03 MPa (1.0 N) and then slowly unloaded to 0.01 MPa, which was set as the zero point. Constant strain-rate (7.6×10^{-4} s^{-1}) stress-relaxation tests were performed to 10 percent compressive strain using a servo-hydraulic machine (model 858, MTS Corp., Minneapolis, MN). Compressive force was measured with a load cell whose sensitivity and range were 0.05 N and 50 N, respectively. Axial displacement was measured with a sensitive linear voltage displacement transducer (LVDT) connected in parallel to the loading shaft. The sensitivity and range of the LVDT were 0.001 mm and 0.6 mm,

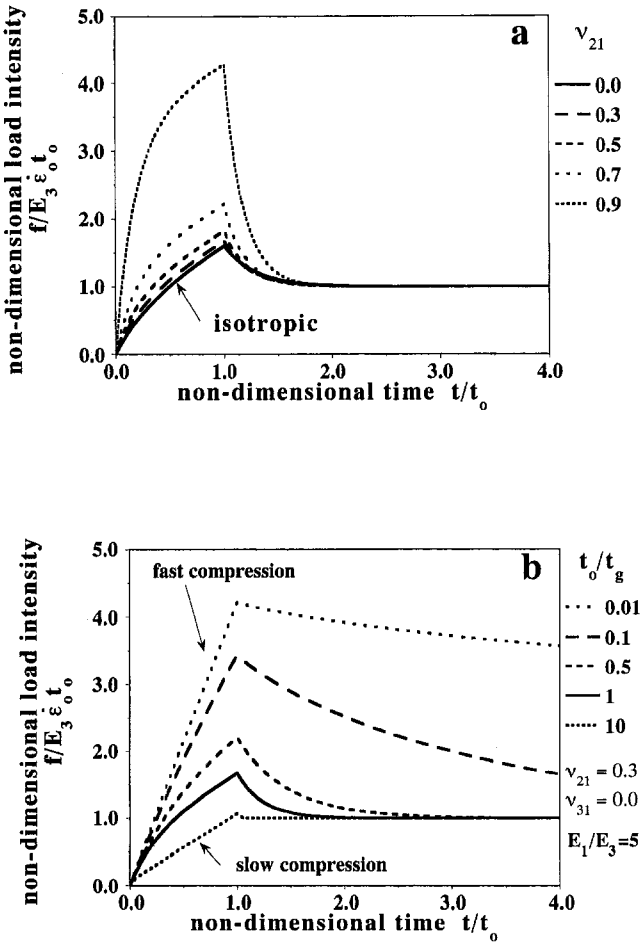

Fig. 4 Stress-relaxation time history in response to a ramped displacement, where $\nu_{31} = 0$: (*a*) The effect of ν_{21} where $E_1/E_3 = 5$ and $t_0/t_g = 1$. (*b*) The effect of t_0/t_g where $\nu_{21} = 0.3$ and $E_1/E_3 = 5$.

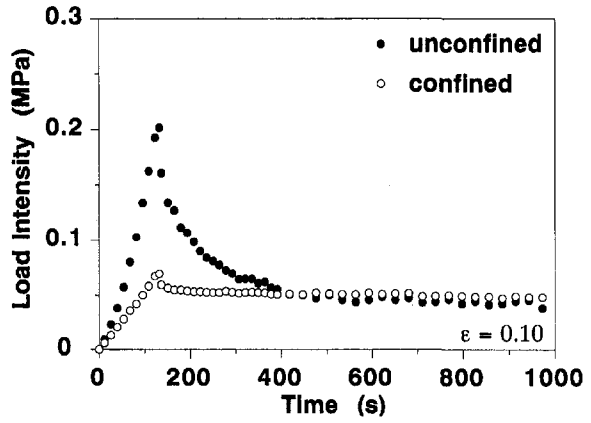

Fig. 5 A typical stress relaxation load intensity time history from confined and unconfined compression tests on GP specimens. Note how the equilibrium responses coincide.

respectively. Throughout the tests, all specimens were bathed in 0.15 M unbuffered NaCl solution containing protease inhibitors (including phenylmethylsulfonyl fluoride).

Results

A typical time history of the load intensity in confined and unconfined compression stress relaxation tests of a GP specimen is shown in Fig. 5. The load intensities at equilibrium (means and standard deviations) are plotted in Fig. 6. A highly significant difference was found between the tissue levels (GP versus CE), but no significant difference was found between the two test types (confined versus unconfined). Furthermore, considering jointly growth plate and chondroepiphysis specimens, sufficient statistical power (>90 percent) exists for an inference that the equilibrium load intensities in the confined and unconfined compression tests are unlikely to differ by more than one standard deviation (paired t-test, $\alpha = 0.05$, $n = 20$). Assuming that the equilibrium load intensities are equal, an immediate consequence of Eqs. (18) and (19) is that $\nu_{31} = 0$ for both GP and CE. Thus, the following procedure was followed in the least-square optimization procedure: First, $\nu_{31} = 0$ was prescribed, and E_3 was given the value f_{eq}/ϵ_0 from the unconfined compression test. Next, the elastic moduli E_1 and ν_{21}, and the permeability k_1 (in the transverse $r-\theta$ plane) were calculated from a three-parameter curve-fit of the unconfined compression results with use of Eqs. (20). The axial permeability k_3 (in the z direction) was obtained from results of the confined compression tests. It can be easily shown that the confined compression displacement field for the transversely isotropic solid matrix is governed by the same equation as that for an isotropic solid matrix with $H_A = C_{33}$. The elastic and permeability coefficients thus obtained for both GP and CE are provided in Table 1.

Table 1 Transversely isotropic biphasic properties of bovine distal ulnar growth plate and chondroepiphysis obtained from confined and unconfined compression tests (means ± std. dev.): (*a*) elastic moduli; (*b*) permeability coefficients

(*a*)	E_3 [MPa] compression	E_1 [MPa] tension	ν_{21}	ν_{31}
Growth plate	0.47 ± 0.11	4.55 ± 1.21	0.30 ± 0.20	0.0
Chondroepiphysis	1.07 ± 0.27	10.63 ± 2.72	0.30 ± 0.26	0.0

(*b*)	k_3 axial [$\times 10^{-15}$ m^4/N-s]	k_1 radial [$\times 10^{-15}$ m^4/N-s]
Growth plate	3.4 ± 1.6	5.0 ± 1.8
Chondroepiphysis	2.1 ± 1.0	4.6 ± 2.1

Significant differences were found in both elastic moduli (E_3 and E_1, $p < 0.01$) and permeability coefficients ($p < 0.05$) between GP and CE (multivariate ANOVA). Growth plate is half as stiff as chondroepiphysis and twice as permeable. Poisson's ratio (ν_{21}) was not significantly different. For comparison, the isotropic model, Eqs. (39) and (40) in Armstrong et al. (1984), was also used to curve-fit the experimental data for one particular specimen. Curve-fits for both the isotropic and transversely isotropic models are given in Fig. 7, in which the biphasic parameters that provided the best fit were: $E_1 = 4.3$ MPa, $E_3 = 0.64$ MPa, $\nu_{31} = 0$, $\nu_{21} = 0.49$, and $k_1 = 5.0 \times 10^{-15}$ m^4/N-s for the transversely isotropic model, and $E = 1.08$ MPa, $\nu = 0$, and $k = 15.5 \times 10^{-15}$ m^4/N-s for the isotropic model. The results indicate that the transversely isotropic model provides a much better fit to the experimental data than an isotropic model. In addition, the optimized solution also yields the required value of the equilibrium load intensity, i.e., $f_{eq} = E_3\epsilon_0$.

Discussion

The transversely isotropic biphasic model provides an excellent description of the stress-relaxation response in the unconfined compression test, where the tissue is under compression in the axial direction and tension in the transverse plane. Previous attempts to model this experiment with isotropic material properties could not produce adequate results, as demonstrated by the inherent maximum theoretical limit of 1.5 on the ratio of the peak to equilibrium load intensity (Armstrong et al., 1984). Using the transversely isotropic model for unconfined compres-

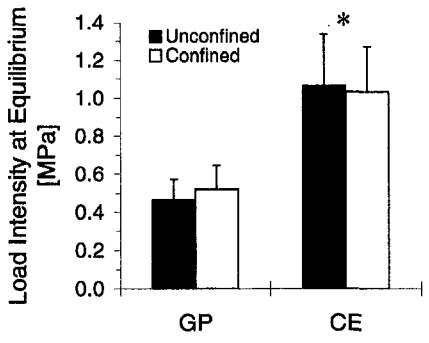

Fig. 6 The load intensity at equilibrium for both growth plate (GP) and chondroepiphysis (CE) in confined and unconfined compression tests (*CE > GP, $p < 0.01$, $n = 10$)

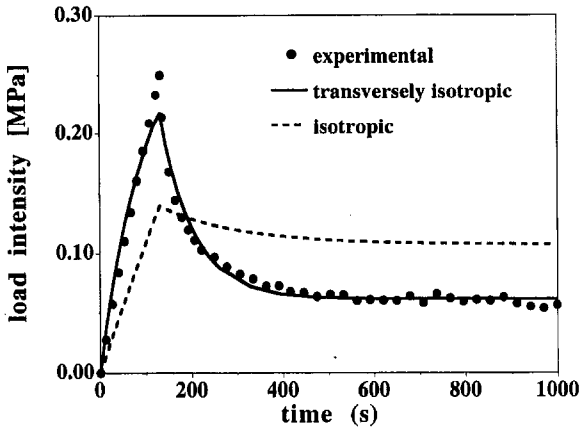

Fig. 7 A typical stress-relaxation time history in response to a ramped displacement (10 percent compression at 131 s) with curve-fits of both isotropic and transversely isotropic biphasic models

sion, where radial expansion (producing tensile strains) is resisted by the fibrous solid matrix, which is stiff in that direction, a high peak load intensity together with a fast stress-relaxation time constant can be attained (e.g., Fig. 4(a)). This stress-relaxation is evident in our own experiments, Fig. 5, as well as in those of Brown and Singerman (1986). The elastic modulus (E_1) in tension (in the transverse plane) is about ten times greater then that in compression (E_3) for both GP and CE, and is similar to the tensile modulus of articular cartilage obtained in specimens parallel to the articular surface (Akizuki et al., 1986).

The linear transversely isotropic biphasic model requires altogether seven constitutive parameters: five elastic constants and two permeability coefficients (in- and out-of-plane). The elastic properties are Young's modulus and Poisson's ratio in the transverse plane (E_1 and ν_{21}, respectively) and out-of-plane (E_3 and ν_{31} respectively) and the out-of-plane shear modulus (G_{31}). In the unconfined compression test, E_3 is in compression, while E_1 is in tension. No shear deformation occurs in our models of confined and unconfined compression; thus the out-of-plane shear modulus, G_{31}, which is an independent material property in transverse isotropy, must be determined separately.

In this study we undertook to limit as much as possible the number of variables determined by curve-fitting the theoretical predictions to the experimental data and thus provide a more robust and unique set of material parameters. Based on the experimental equivalence of the equilibrium stress intensities in confined and unconfined compression, we assumed $\nu_{31} = 0$ as would theoretically result from equating Eqs. (18) and (19). We note, however, that due to experimental variability ν_{31} may range up to 0.2. Nonzero values for ν_{31} have been previously reported for articular cartilage (Woo et al., 1976; Hoch et al., 1983; Mizrahi et al., 1986; Jurvelin et al., 1995).

A significant difference in material properties exists between growth plate and chondroepiphysis of the bovine distal ulna, consistent with the ultrastructural difference between these two tissues. A strong anisotropy is also evident in both tissues. Thus, material inhomogeneity and anisotropy should be considered when analyzing the mechanical behavior in compression of growth plate and chondroepiphysis.

Acknowledgments

This study was supported by a gift from the St. Giles Foundation, Brooklyn, NY.

References

Akizuki, S., Mow, V. C., Muller, F., Pita, J. C., Howell, D. S., and Manicourt, D. H., 1986, "Tensile Properties of Human Knee Joint Cartilage: I. Influence of Ionic Conditions, Weight Bearing and Fibrillation on the Tensile Modulus," *J. Orthop. Res.*, 4:379–392.

Armstrong, C. G., Lai, W. M., and Mow, V. C., 1984, "An Analysis of the Unconfined Compression of Articular Cartilage," ASME JOURNAL OF BIOMECHANICAL ENGINEERING, 106:165–173.

Bright, R. W., Burstein, A. H., and Elmore, S. M., 1974, "Epiphyseal Plate Cartilage: A Biomechanical and Histological Analysis of Failure Modes," *J. Bone Joint Surg.*, 56A:688–703.

Brighton, C. T., 1978, "Structure and Function of the Growth Plate," *Clin. Orthop. Rel. Res.*, 136:22–32.

Brown, T. D., and Singerman, R. J., 1986, "Experimental Determination of the Linear Biphasic Constitutive Coefficients of Human Fetal Proximal Femoral Chondroepiphysis," *J. Biomech.*, 19:597–605.

Buckwalter, J. A., Mower, D., Schafer, J., Ungar, R., Ginsberg, B., and Moore, K., 1985, "Growth-Plate Chondrocyte Profiles and Their Orientation," *J. Bone Joint Surg.*, 67A:942–955.

Carter, D. R., Orr, T. E., Fyhrie, D. P., and Schurman, D. J., 1987, "Influences of Mechanical Stress on Prenatal and Postnatal Skeletal Development," *Clin. Orthop. Rel. Res.*, 219:237–250.

Cohen, B., 1992, "Anisotropic Hydrated Soft Tissues in Finite Deformation and the Biomechanics of the Growth Plate," Ph.D. thesis, Columbia University, New York.

Cohen, B., Chorney, G. S., Phillips, D. P., Dick, H. M., and Mow, V. C., 1992, "Inhomogeneous and Anisotropic Mechanical Properties of Bovine Growth Plate and Chondroepiphysis," *Trans. Orthop. Res. Soc.*, 17:153.

Cohen, B., Chorney, G. S., Phillips, D. P., Dick, H. M., and Mow, V. C., 1994, "Compressive Stress-Relaxation Behavior of Bovine Growth Plate May Be Described by the Nonlinear-Biphasic Theory," *J. Orthop. Res.*, 12:804–813.

Gray, M. L., Pizzanelli, A. M., Grodzinsky, A. J., and Lee, R. C., 1988, "Mechanical and Physicochemical Determinants of the Chondrocyte Biosynthetic Response," *J. Orthop. Res.*, 6:777–792.

Hoch, D. H., Grodzinsky, A. J., Koob, T. J., Albert, M. L., and Eyre, D. R., 1983, "Early Changes in Material Properties of Rabbit Articular Cartilage After Menisectomy," *J. Orthop. Res.*, 1:4–12.

Hunziker, E. B., Schenk, R. K., and Cruz-Orive, L.-M., 1987, "Quantitation of Chondrocyte Performance in Growth Plate Cartilage During Longitudinal Bone Growth," *J. Bone Joint Surg.*, 69A:162–173.

Jones, R. M., 1975, *Mechanics of Composite Materials*, Scripta, Washington, DC.

Jurvelin, J. S., Buschmann, M. D., and Hunziker, E. B., 1995, "Characterization of the Equilibrium Response of Bovine Humeral Cartilage in Confined and Unconfined Compression," *Trans. Orthop. Res. Soc.*, 20:512.

Kim, Y. J., Bonassar, L. J., and Grodzinsky, A. J., 1995, "The Role of Cartilage Streaming Potential, Fluid Flow and Pressure in the Stimulation of Chondrocyte Biosynthesis During Dynamic Compression," *J. Biomech.*, 28:1055–1066.

Lai, W. M., and Mow, V. C., 1980, "Drag Induced Compression of Articular Cartilage During a Permeation Experiment," *Biorheology*, 17:111–123.

Lanir, Y., 1987, "Biorheology and Fluid Flux in Swelling Tissues II. Analysis of Unconfined Compressive Response of Transversely Isotropic Cartilage Disc," *Biorheology*, 24:189–205.

Letts, R. M., 1988, "Compression Injuries of the Growth Plate," in: *Behavior of the Growth Plate*, Uhthoff, H. K., and Wiley, J. J., eds., Raven Press, New York, pp. 111–118.

Mak, A. F., 1986, "Unconfined Compression of Hydrated Viscoelastic Tissues: A Biphasic Poroviscoelastic Analysis," *Biorheology*, 23:371–383.

Mak, A. F., Lai, W. M., and Mow, V. C., 1987, "Biphasic Indentation of Articular Cartilage: I. Theoretical Analysis," *J. Biomech.*, 24:587–597.

Mizrahi, J., Maroudas, A., Lanir, Y., Ziv, I., and Webber, T. J., 1986, "The Instantaneous Deformation of Cartilage: Effects of Collagen Fiber Orientation and Osmotic Stress," *Biorheology*, 23:311–330.

Moen, C. T., and Pelker, R. R., 1984, "Biomechanical and Histological Correlations in Growth Plate Failure," *J. Pediat. Orthop.*, 4:180–184.

Mow, V. C., Kuei, S. C., Lai, W. M., and Armstrong, C. G., 1980, "Biphasic Creep and Stress Relaxation of Articular Cartilage: Theory and Experiments," ASME JOURNAL OF BIOMECHANICAL ENGINEERING, 102:73–84.

Smith, J. W., 1962, "The Relationship of Epiphysial Plates to Stress in Some Bones of the Lower Limb," *J. Anat.*, 96:58–78.

Speer, D. P., 1982, "Collagenous Architecture of the Growth Plate and Perichondrial Ossification Groove," *J. Bone Joint Surg.*, 64A:399–407.

Spilker, R. L., and Suh, J.-K., 1990, "Formulation and Evaluation of a Finite Element Model for the Biphasic Model of Hydrated Soft Tissues," *Computers and Structures*, 35:425–439.

Spilker, R. L., Suh, J.-K., Mow, V. C., 1990, "Effects of Friction on the Unconfined Compressive Response of Articular Cartilage: A Finite Element Analysis," ASME JOURNAL OF BIOMECHANICAL ENGINEERING, 112:138–149.

Woo, S. L.-Y., Akeson, W. H., and Jemmott, G. F., 1976, "Measurements of Nonhomogeneous and Directional Mechanical Properties of Articular Cartilage in Tension," *J. Biomech.*, 9:785–791.

Yang, M., and Taber, L. A., 1991, "The Possible Role of Poroelasticity in the Apparent Viscoelastic Behavior of Passive Cardiac Muscle," *J. Biomech.*, 24:587–597.